SIAM J. SCI. COMPUT.
Vol. 41, No. 5, pp. A2772–A2794

A FOURIER EXTENSION BASED NUMERICAL INTEGRATION SCHEME FOR FAST AND HIGH-ORDER APPROXIMATION OF CONVOLUTIONS WITH WEAKLY SINGULAR KERNELS*

AKASH ANAND† AND AWANISH K. TIWARI†

Abstract. Computationally efficient numerical methods for high-order approximations of convolution integrals involving weakly singular kernels find many practical applications including those in the development of fast quadrature methods for numerical solution of integral equations. Most fast techniques in this direction utilize uniform grid discretizations of the integral that facilitate the use of FFT for $O(n \log n)$ computations on a grid of size n. In general, however, the resulting error converges slowly with increasing n when the integrand does not have a smooth periodic extension. Such extensions, in fact, are often discontinuous, and, therefore, their approximations by truncated Fourier series suffer from Gibbs oscillations. In this paper, we present and analyze an $O(n \log n)$ scheme, based on a Fourier extension approach for removing such unwanted oscillations, that not only converges with high order but is also relatively simple to implement. We include a theoretical error analysis as well as a wide variety of numerical experiments to demonstrate its efficacy.

Key words. Fourier extension, singular function, quadrature method, convolution, high order, scattering problem

AMS subject classifications. 65D15, 65R10, 65T40, 44A35

DOI. 10.1137/18M1232826

1. Introduction.

In this paper, we consider the problem of approximating the integral operator $A : C([0,1]) \to C([0,1])$ given by

$$(Au)(x) = \int_0^1 g(x-y)u(y)dy \tag{1.1}$$

with a weakly singular kernel g using a numerical integration scheme of the form

$$(A_n u)(x) = \sum_{j=0}^{n} w_j^n(x) u(x_j^n) \tag{1.2}$$

with quadrature points $x_j^n = j/n$ and weights $w_j^n(x)$ that depend on the kernel g. The primary aim of this effort is to develop a quadrature so that the approximations in (1.2) (a) converge with high order, that is, for all $u \in C^r([0,1])$, satisfy

$$\|A_n u - Au\|_\infty \leq C(u) n^{-\nu(r)}$$

for some increasing and positive function $\nu : \mathbb{N} \to \mathbb{R}^+$, and (b) can be evaluated at quadrature points efficiently, that is, the set $\{(A_n u)(x_j^n) : j = 0, \ldots, n\}$ can be computed in $O(n \log n)$ operations.

*Submitted to the journal's Methods and Algorithms for Scientific Computing section December 13, 2018; accepted for publication (in revised form) June 24, 2019; published electronically September 10, 2019.

https://doi.org/10.1137/18M1232826

Funding: This work was supported by ISRO-IITK Space Technology Cell through file STC/MATH/2014100 and by the Science & Engineering Research Board through file MTR/2017/000643.

†Department of Mathematics and Statistics, Indian Institute of Technology Kanpur, Kanpur, Uttar Pradesh, 208016, India (akasha@iitk.ac.in, awanishtk@gmail.com).

For example, such a quadrature can then be utilized toward obtaining an $O(n \log n)$ Nyström solver for numerical solution of integral equations of the form

$$u(x) - \int_0^1 g(x-y)m(y)u(y)\,dy = f(x), \quad x \in [0,1]$$

for $f, m \in C^r([0,1])$.

While several numerical integration schemes for integrands that have a point singularity within the domain of integration have been developed, this problem remains an active area of research. In the special case when the integrand singularity is at one or both endpoints of the interval, an appropriate change of variable, as suggested by Kress in [34], can be employed for their analytical resolution, where a subsequent use of trapezoidal rule yields a high-order numerical accuracy. The more general case where the singularity is an interior point of the interval requires more careful treatment. Among the available techniques, a prominent example is a high-order corrected trapezoidal rule due to Rokhlin [41]. While a rapid increase in the magnitude of correction weights with increasing order limits their original approach to low-order convergence rates, Rokhlin together with Kapur subsequently introduced another scheme (see [32]) that handles the singularity by separating the integrand into regular and singular parts along with allowing some quadrature nodes to lie outside the interval of integration. In this case, however, the linear system for determining the nodes and weights, especially near the interval endpoints, is poorly conditioned and worsens rapidly with increasing order.

In a subsequent effort, Alpert [6] introduced a hybrid Gauss-trapezoidal rule that is based on the periodic trapezoidal rule. In this scheme, Alpert replaced the equispaced nodes near each end with an optimal set of auxiliary nodes that are chosen using the algorithm of Kolm and Rokhlin [33]. Later, based on a combination of boundary and singularity correction, Aguilar and Chen proposed a corrected trapezoidal rule for logarithmic singularity in $\mathbb{R}^2$ [2] and for the singularity of the form $1/|x|$ in $\mathbb{R}^3$ [3]. While they numerically demonstrated the effectiveness of this scheme in computing singular integrals, a corresponding convergence analysis is not readily available.

More recently, Duan and Rokhlin [14] introduced a class of quadrature formulae for handling singularities of the form $\log|x|$ in two dimensions and $1/|x|$ in three dimensions. This approach is somewhat related to the Ewald summation [16] and leads to quadratures that can be viewed as a version of the corrected trapezoidal rule. To avoid solving ill-conditioned linear systems for obtaining the quadrature weights, the scheme uses very lengthy analytic expressions that depend on the underlying mesh. A recent paper in this direction by Marin, Runborg, and Tornberg [36] is again a corrected trapezoidal approach, where singular functions of the form $|x|^\gamma$, $\gamma > -1$ in one dimension and $|x|^{-1}$ in two dimensions were considered for high-order numerical integration.

In an attempt that is somewhat similar in spirit to the proposed scheme, Xu, Austin, and Wei [43] presented a fast algorithm to compute the convolution using Fourier extensions. However, unlike the problem attempted in this paper, their methodology is aimed toward computing the convolutions of two compactly supported functions and only achieves a computational complexity of $O(n(\log n)^2)$. For the construction of Fourier extension, they employ an algorithm, due to Matthysen and Huybrechs [37], that relies on solving a least-squares minimization problem using randomized techniques and exploits the rapid decay of the singular values of the associated matrix in $O(n(\log n)^2)$ operations.

The scheme introduced in this paper utilizes a regular grid in order to employ the fast Fourier transform (FFT) to obtain convolution values in $O(n \log n)$ computational

time. Indeed, as

$$(Au)(x) = \sum_{k=-\infty}^{\infty} \widehat{g_e}(k)\widehat{u_e}(k)e^{2\pi ikx}, \tag{1.3}$$

where g_e and u_e denote the periodic extension of g and u, respectively, and for 1-periodic function v, $\hat{v}$ denotes its Fourier coefficients given by

$$\hat{v}(k) = \int_0^1 v(x)e^{-2\pi ikx}\,dx,$$

the inverse FFT evaluates the truncated series

$$(A_n u)(x_j^n) = \sum_{k=-n/2}^{n/2-1} \widehat{g_e}(k)\widehat{u_e}(k)e^{2\pi ikx_j^n}$$

at $x_j^n, j = 0, \ldots, n-1$ in a straightforward manner in $O(n \log n)$ operations. However, in general, the resuting error

$$\|Au - A_n u\|_\infty \leq \sum_{|k|\geq n/2} |\widehat{g_e}(k)||\widehat{u_e}(k)|$$

converges slowly with increasing n owing to discontinuous u_e and singular g_e. In this paper, we suggest an approach to alleviate the difficulty of slow convergence by making u_e more amenable to Fourier approximation that also allows us to precompute the Fourier coefficients for g_e more accurately resulting in an overall rapidly convergent numerical integration scheme.

The organization of the paper is as follows. In section 2, we describe the construction of Fourier extension for smooth functions where the functional data is available on equispaced grids. Next, in section 3, we provide the proposed numerical integration scheme for the approximation of the convolution A. We then present a theoretical analysis of our integration scheme in section 4. In section 5, we present the numerical computation of singular moments that occur in the numerical integration scheme. Further, as a special case, we discuss our numerical integration scheme for a compactly supported function in section 6. A variety of numerical results to validate the accuracy of our quadrature implemented in this paper are presented in section 7.

2. Fourier extension. We consider the problem of approximation of a function $u \in C^\infty([0,1])$ by a truncated Fourier series where discrete functional data is available on an equispaced grid on the interval $[0,1]$. Recall that the Fourier series approximations fail to converge uniformly when $u(0) \neq u(1)$ due to rapid oscillations near the boundary, known as the Gibbs phenomenon [21, 22, 29, 42]. Several approximation approaches have been proposed to overcome the difficulty of Gibbs oscillations. These include schemes that utilize Fourier or physical space filters [27] as well as those that project the partial Fourier sums onto suitable functional spaces. For example, the Gegenbauer projection technique [23, 24, 25, 26, 27, 28] utilizes a space spanned by Gegenbauer polynomials. In Fourier–Padé approximations, partial Fourier sums are approximated by rational trigonometric functions [13, 19, 20]. Techniques based on extrapolation algorithms [9] have also been used. Several Fourier extension ideas have also been proposed that seek to find a trigonometric polynomial of the form

$$\sum_{k=-n}^{n-1} \widehat{u_{c,e}}(k)e^{2\pi ikx/b}$$

with $b \geq 1$, where $u_{c,e}$ is the b-periodic extension of u_c, the continuation of u on $[0,1]$ to u_c on $[0,b]$ or $[1-b,1]$ in such a way that $u_c \equiv u$ on $[0,1]$. In addition, it is desirable that $u^{(\ell)}(0) = u_c^{(\ell)}(b)$ for all integers $0 \leq \ell \leq r$, for some $r \geq 0$, is satisfied in order to control the decay rate of Fourier coefficients. Once such a u_c has been produced, the restriction of its truncated Fourier series to $[0,1]$ serves as an approximation to u. For some examples where Fourier extension ideas have been used and discussed in various contexts including their stability, applicability in PDE solvers, and surface representations, see [1, 4, 5, 7, 8, 11, 12, 15, 17, 18, 30, 35, 37, 38, 39, 40]. In particular, albeit in different contexts, the extension in [17, 18, 40] uses a polynomial based approach, much like the one we review below and employ in the proposed integration scheme. However, before doing so, we must mention that while we restrict our presentation and analysis to the polynomial based extension, utilizing other construction ideas, for instance, Fourier continuation based on Gram polynomials in [11], in the context of computing convolutions should also be possible. These could be interesting future explorations in terms of accessing their relative performance.

In the present context, a grid of size $n+1$ has its jth grid point at $x_j = j/n$, where the corresponding function value $u(x_j)$ is assumed to be known and is denoted by u_j for $j = 0, \ldots, n$. The function u is continued to the interval $[-1,1]$ as

$$u_c(x) = \begin{cases} u(x), & x \in [0,1], \\ p(U)(x), & x \in [-1,0), \end{cases} \tag{2.1}$$

where, for a $2 \times (r+1)$ matrix $U = (u_{ij})_{0 \leq i \leq 1, 0 \leq j \leq r}$, $p(U)$ is a polynomial of degree $2r+1$ of the form

$$p(U)(x) = \sum_{m=0}^{r} u_{0m}\, p_m^0(x) + \sum_{m=0}^{r} u_{1m}\, p_m^1(x) \tag{2.2}$$

with

$$p_m^0(x) = \frac{1}{m!} x^m (1+x)^{r+1} \sum_{n=0}^{r-m} (-x)^n \binom{r+n}{n}$$

and

$$p_m^1(x) = \frac{1}{m!} (1+x)^m (-x)^{r+1} \sum_{n=0}^{r-m} (1+x)^n \binom{r+n}{n}.$$

It is easy to check that, for $0 \leq m \leq r$, the mth derivative of the polynomial $p(U)$ satisfies

$$p(U)^{(m)}(0) = u_{0m}, \quad p(U)^{(m)}(-1) = u_{1m}.$$

Thus, choosing the entries of U as

$$u_{0m} = u^{(m)}(0) \quad \text{and} \quad u_{1m} = u^{(m)}(1)$$

ensures that $u_c \in C^r([-1,1])$. The continued discrete data $(u_c)_j = u_c(j/n), j = -n, \ldots, n-1$ is then used to obtain

$$\hat{u}_{c,n}(k) = \frac{1}{2n} \sum_{j=-n}^{n-1} (u_c)_j\, e^{-\pi i j k/n} \tag{2.3}$$

for $k = -n, \ldots, n-1$, to arrive at the interpolating Fourier extension approximation for the discrete problem given by

$$u_{c,n}(x) = \sum_{k=-n}^{n-1} \hat{u}_{c,n}(k) e^{\pi i k x}. \tag{2.4}$$

However, in general, the derivative data $u^{(m)}(0)$ and $u^{(m)}(1)$ may not be available exactly, and their approximations need to be obtained using the discrete data u_j. In such a scenario, we replace U by its approximation U^q with entries obtained as $u^q_{00} = u(x_0)$, $u^q_{10} = u(x_n)$, and for $1 \le m \le r$, we set

$$u^q_{0m} = \mathcal{D}^{m,+}_{n,q}(u)(x_0) \text{ and } u^q_{1m} = \mathcal{D}^{m,-}_{n,q}(u)(x_n),$$

using forward and backward difference operators $\mathcal{D}^{m,+}_{n,q}(u)$ and $\mathcal{D}^{m,-}_{n,q}(u)$, respectively, of the order of accuracy q as approximations of $u^{(m)}$ whose generic form reads

$$D^{m,\pm}_{n,q}(u)(x_\ell) = (\pm n)^m \left(\sum_{k=0}^{m+q-1} \left(a^m_q\right)_k u_{\ell \pm k} \right)$$

for appropriately chosen constants $\left(a^m_q\right)_k$. The continuation of u corresponding to the boundary data matrix U^q is denoted by u^q_c. The continued data $(u^q_c)_j = u^q_c(j/n), j = -n, \ldots, n-1$ is then used to similarly obtain

$$\hat{u}^q_{c,n}(k) = \frac{1}{2n} \sum_{j=-n}^{n-1} \left(u^q_c\right)_j e^{-\pi i j k/n} \tag{2.5}$$

for $k = -n, \ldots, n-1$ and the corresponding Fourier extension approximation given by

$$u^q_{c,n}(x) = \sum_{k=-n}^{n-1} \hat{u}^q_{c,n}(k) e^{\pi i k x}. \tag{2.6}$$

Note that the coefficients $\hat{u}^q_{c,n}(k)$ can be computed in $\mathcal{O}(n \log n)$ computational time using the FFT. We use the approximation $u^q_{c,n}$ of u to construct a numerical integration scheme A_n, which we discuss next.

3. The integration scheme. We begin by observing that

$$(Au)(x) = \int_0^1 g(x-y)u(y)\,dy = \int_0^1 g(x-y)u_c(y)\,dy,$$

where u_c is the continuation of u to $[-1, 1]$ as described in the previous section. We rewrite Au as

$$(Au)(x) = \int_{x-1}^{x+1} g(x-y)u_c(y)dy - (C_L U)(x) - (C_R U)(x),$$

where C_L and C_R are given by

$$(C_L U)(x) = \int_{x-1}^{0} g(x-y)p(U)(y)dy,$$
$$(C_R U)(x) = \int_{1}^{x+1} g(x-y)p(U)(y-2)dy.$$

The Fourier series for the 2-periodic extension $u_{c,e}$ of u_c can then be utilized to write the integral as

$$(Au)(x) = \sum_{k=-\infty}^{\infty} \mathcal{G}(k)\widehat{u_{c,e}}(k)e^{\pi ikx} - (C_L U)(x) - (C_R U)(x), \tag{3.1}$$

where

$$\widehat{u_{c,e}}(k) = \frac{1}{2}\int_{x-1}^{x+1} u_c(y)e^{-\pi iky}\,dy$$

and

$$\mathcal{G}(k) = \int_{-1}^{1} g(\rho)e^{\pi ik\rho}\,d\rho. \tag{3.2}$$

In view of this, we take the numerical integration scheme A_n to be of the form

$$(A_n u)(x) = \sum_{k=-n}^{n-1} \mathcal{G}(k)\hat{u}^q_{c,n}(k)e^{\pi ikx} - (C_L U^q)(x) - (C_R U^q)(x). \tag{3.3}$$

We note that the scheme does not require constructing a periodic extension for g toward obtaining $\mathcal{G}(k)$. The functions $(C_L U)(x)$ and $(C_R U)(x)$, the left and right corrections in (3.3), can be obtained from analytical expressions easily derived using the form of continuation polynomial. In particular,

$$(C_L U)(x) = \int_{x-1}^{0} g(x-y)p(U)(y)\,dy = \sum_{m=0}^{r} u_{0m}\ \mu_m^{L,0}(x) + \sum_{m=0}^{r} u_{1m}\mu_m^{L,1}(x),$$

where $\mu_m^{L,j}(x) = \int_x^1 g(y)p_m^j(x-y)\,dy$, $j = 0, 1$. These can be further expanded in terms of the moments ν_k^L given by

$$\nu_k^L(x) = \int_x^1 y^k g(y)\,dy.$$

In many interesting instances, these moments are known analytically. For example, if $g(x) = |x|^\gamma$, then we have $\nu_k^L(x) = \left(1 - x^{k+1+\gamma}\right)/(k+1+\gamma)$, and when $g(x) = \log|x|$,

$$\nu_k^L(x) = \frac{-x^{k+1}\log|x|}{k+1} - \frac{1-x^{k+1}}{(k+1)^2}.$$

Indeed, $\mu_m^{L,0}(x)$ and $\mu_m^{L,1}(x)$ are given by

$$\frac{1}{m!}\sum_{n=0}^{r-m}\binom{r+n}{n}\sum_{q=0}^{r+1}\binom{r+1}{q}\sum_{k=0}^{m+n+q}(-1)^{n+k}\binom{m+n+q}{k}x^{m+n+q-k}\nu_k^L(x)$$

and

$$\frac{1}{m!}\sum_{n=0}^{r-m}\binom{r+n}{n}\sum_{q=0}^{m+n}\binom{m+n}{q}\sum_{k=0}^{r+q+1}(-1)^{r+1+k}\binom{r+q+1}{k}x^{r+q+1-k}\nu_k^L(x),$$

respectively. A similar calculation yields

$$(C_R U)(x) = \int_1^{x+1} g(x-y)p(U)(y-2)\,dy = \sum_{m=0}^{r} u_{0m}\ \mu_m^{R,0}(x) + \sum_{m=0}^{r} u_{1m}\mu_m^{R,1}(x)$$

with $\mu_m^{R,0}(x)$ and $\mu_m^{R,1}(x)$ given by

$$\frac{1}{m!}\sum_{n=0}^{r-m}\binom{r+n}{n}\sum_{q=0}^{r+1}\binom{r+1}{q}\sum_{k=0}^{m+n+q}(-1)^{n+k}\binom{m+n+q}{k}(x-2)^{m+n+q-k}\nu_k^R(x)$$

and

$$\frac{1}{m!}\sum_{n=0}^{r-m}\binom{r+n}{n}\sum_{q=0}^{m+n}\binom{m+n}{q}\sum_{k=0}^{r+q+1}(-1)^{r+1+k}\binom{r+q+1}{k}(x-2)^{r+q+1-k}\nu_k^R(x),$$

respectively, where

$$\nu_k^R(x)=\int_{1-x}^{1}y^k g(y)\,dy.$$

Interestingly, these calculations imply that the corrections can be computed on a grid of size n in $O(n)$ operations and do not adversely impact the overall computational complexity of $O(n\log n)$.

Remark 3.1. Clearly, obtaining $(A_n u)(x_j), j=0,\dots,n$, requires computing corresponding corrections $(C_L U)(x_j)$ and $(C_R U)(x_j)$ which, in turn, demand that moments $\nu_k^L(x)$ and $\nu_k^R(x)$ be available at $x=x_j, j=0,\dots,n$. As mentioned above, for a certain class of weakly singular kernels, these are available analytically. More generally when these are not available analytically, they can be obtained in $O(n)$ operations through integrals of the form

$$\int_{x_j}^{1}y^k g(y)\,dy$$

for $k=0,\dots,2r+1$, which can be computed numerically to a high level of accuracy using a fixed number of quadrature points independent of the computational grid, thus preserving the overall $O(n\log n)$ computational complexity of the proposed approach.

The numerical schemes (3.3) can be rewritten in the form of a quadrature on the equispaced grid given by

$$(A_n u)(x)=\sum_{j=0}^{n}w_j^n(x)u(x_j^n) \tag{3.4}$$

with quadrature points $x_j^n=j/n$ and weights $w_j^n(x)=\mathfrak{w}_j^n(x)+\mathfrak{c}_j^n(x)$ where, for $-n+1\le\ell\le n$,

$$\mathfrak{w}_\ell^n(x)=\frac{1}{2n}\sum_{k=-n}^{n-1}\mathcal{G}(k)e^{\pi ik(x-\ell/n)}$$

and

$$\mathfrak{c}_j^n(x)=\begin{cases}\displaystyle\sum_{m=\max\{0,j-q+1\}}^{r}n^m\left(a_q^m\right)_j\chi_m^0(x), & 0\le j\le r+q-1,\\ \displaystyle\sum_{m=\max\{0,j-q+1\}}^{r}(-n)^m\left(a_q^m\right)_{n-j}\chi_m^1(x), & n-(r+q-1)\le j\le n,\\ 0 & \text{otherwise}\end{cases}$$

with

$$\chi_m^k(x) = \sum_{\ell=-n+1}^{-1} p_m^k(\ell/n)\mathfrak{w}_\ell(x) - \left(\mu_m^{L,k}(x) + \mu_m^{R,k}(x)\right).$$

In writing the corrections $\mathfrak{c}_j^n$, for simplicity, we have assumed that n is large enough so that $r+q-1 < n/2$ is satisfied; otherwise, left and right corrections overlap for $n-(r+q-1) \le j \le r+q-1$ and $\mathfrak{c}_j^n(x)$ is given by

$$\mathfrak{c}_j^n(x) = \sum_{m=\max\{0,j-q+1\}}^{r} n^m \left(\left(a_q^m\right)_j \chi_m^0(x) + (-1)^m \left(a_q^m\right)_{n-j} \chi_m^1(x) \right).$$

Note that while (3.3) provides an $O(n \log n)$ scheme for obtaining the convolution on an equispaced grid on size n, one could use (3.4) with the precomputed weights for a single point integration. Use of either form requires the values $\mathcal{G}(k)$ that, in principle, can be obtained exactly through the symbolic integration of (3.2). In practice, however, it might be more convenient to numerically precompute them to high precision and store them for later calculations. We discuss a couple of numerical strategies toward this in section 5.

In the next section, we investigate the errors that are associated with the proposed numerical scheme.

4. Error analysis. Clearly, from (3.1) and (3.3), the error in the numerical scheme is given by

$$\begin{aligned}(Au)(x) - (A_n u)(x) = \\ \sum_{k=-n}^{n-1} \mathcal{G}(k) \left(\widehat{u_{c,e}}(k) - \hat{u}_{c,n}(k)\right) e^{\pi i k x} + \sum_{\substack{k\ge n \\ k<-n}} \mathcal{G}(k)\widehat{u_{c,e}}(k) e^{\pi i k x} + \\ \sum_{k=-n}^{n-1} \mathcal{G}(k) \left(\hat{u}_{c,n}(k) - \hat{u}_{c,n}^q(k)\right) e^{\pi i k x} - (C_L(U-U^q))(x) - (C_R(U-U^q))(x). \end{aligned} \tag{4.1}$$

To estimate the magnitude of

$$\sum_{k=-n}^{n-1} \mathcal{G}(k) \left(\widehat{u_{c,e}}(k) - \hat{u}_{c,n}(k)\right) e^{\pi i k x} + \sum_{\substack{k\ge n \\ k<-n}} \mathcal{G}(k)\widehat{u_{c,e}}(k) e^{\pi i k x},$$

we recall that $\mathcal{G}(k) = \mathcal{G}(-k)$ and

$$\hat{u}_{c,n}(k) - \widehat{u_{c,e}}(k) = \sum_{\ell=1}^{\infty} \left(\widehat{u_{c,e}}(k+2\ell n) + \widehat{u_{c,e}}(k-2\ell n)\right)$$

to arrive at the upper bound

$$\sum_{k=-n}^{n-1} |\mathcal{G}(k)| \sum_{\ell=1}^{\infty} |\widehat{u_{c,e}}(k+2\ell n) + \widehat{u_{c,e}}(-k-2\ell n)| + \sum_{|k|\ge n} |\mathcal{G}(k)||\widehat{u_{c,e}}(k) + \widehat{u_{c,e}}(-k)|. \tag{4.2}$$

We also observe that, for $x \in [0,1]$, we have

$$(C_L(U-U^q))(x) + (C_R(U-U^q))(x) = \sum_{\ell=-\infty}^{\infty} \mathcal{G}(k)\widehat{(u_{c,e}-u_{c,e}^q)}(k)e^{\pi ikx},$$

and, therefore, we get

$$(C_L(U-U^q))(x) + (C_R(U-U^q))(x) - \sum_{k=-n}^{n-1} \mathcal{G}(k)\left(\hat{u}_{c,n}(k) - \hat{u}_{c,n}^q(k)\right) =$$
$$\sum_{k=-\infty}^{\infty} \mathcal{G}(k)\widehat{(u_{c,e}-u_{c,e}^q)}(k)e^{\pi ikx} - \sum_{k=-n}^{n-1} \mathcal{G}(k) \sum_{\ell=-\infty}^{\infty} \widehat{(u_{c,e}-u_{c,e}^q)}(k+2\ell n) =$$
$$- \sum_{k=-n}^{n-1} \mathcal{G}(k) \sum_{\substack{\ell=-\infty \\ \ell\neq 0}}^{\infty} \widehat{(u_{c,e}-u_{c,e}^q)}(k+2\ell n) + \sum_{\substack{k\geq n \\ k<-n}} \mathcal{G}(k)\widehat{(u_{c,e}-u_{c,e}^q)}(k)e^{\pi ikx}.$$

Thus, its magnitude can be bounded above by

$$\sum_{k=-n}^{n-1} |\mathcal{G}(k)| \sum_{\ell=1}^{\infty} |\widehat{(u_{c,e}-u_{c,e}^q)}(k+2\ell n) + \widehat{(u_{c,e}-u_{c,e}^q)}(-k-2\ell n)| +$$
$$\sum_{|k|\geq n} |\mathcal{G}(k)||\widehat{(u_{c,e}-u_{c,e}^q)}(k)|. \tag{4.3}$$

We make note of the following useful estimate for the numerical scheme error.

LEMMA 4.1. *Let $g : \mathbb{R} \to \mathbb{R}$ be an even and absolutely integrable function for $u \in C([0,1])$, $u_{c,e}$ be the 2-periodic extension of u_c as defined in (2.1), $u_{c,e}^q$, $q \in \mathbb{N}$ be as given in (2.4), and let the sequence of approximations $A_n, n \in \mathbb{N}$ as defined in (3.4) to A in (1.1). Then, for all $u \in C([0,1])$, we have the estimate*

$$\|Au - A_n u\|_\infty \leq$$
$$\sum_{|k|\geq n} |\mathcal{G}(k)||\widehat{u_{c,e}}(k) + \widehat{u_{c,e}}(-k)| + \sum_{|k|\geq n} |\mathcal{G}(k)||\widehat{(u_{c,e}-u_{c,e}^q)}(k)| +$$
$$\sum_{k=-n}^{n-1} |\mathcal{G}(k)| \sum_{\ell=1}^{\infty} |\widehat{u_{c,e}}(k+2\ell n) + \widehat{u_{c,e}}(-k-2\ell n)| +$$
$$\sum_{k=-n}^{n-1} |\mathcal{G}(k)| \sum_{\ell=1}^{\infty} |\widehat{(u_{c,e}-u_{c,e}^q)}(k+2\ell n) + \widehat{(u_{c,e}-u_{c,e}^q)}(-k-2\ell n)|.$$

The convergence rate, therefore, depends not only on the regularity of u and the order of derivative approximations q but also on the decay rate of $\mathcal{G}(k)$. The convergence, however, does not depend on the decay of $\mathcal{G}(k)$ as can be seen from the proof of Theorem 4.5. We make the following observations on the decay rates of $\mathcal{G}$.

For weakly singular kernels $g(x)$, we have the following result.

PROPOSITION 4.2. *For a $\gamma \in (-1, \infty)$ and weakly singular kernels $g(x)$, there exists a positive constant B_γ such that*

$$|\mathcal{G}(k)| \leq B_\gamma |k|^{-\min\{1+\gamma, 2\}}$$

for all $k \neq 0$.

Proof. We begin by proving the result for $g(x) = |x|^\gamma, \gamma \in (-1, \infty)$. Note that we only need to show that the result holds for $k > 0$ as $\mathcal{G}(-k) = \overline{\mathcal{G}(k)}$. We first assume that $\gamma \in (-1, 0)$, $k > 0$, and observe that

$$\mathcal{G}(k) = \frac{2}{k^{1+\gamma}} \vartheta(k), \tag{4.4}$$

where

$$\vartheta(k) = \sum_{\ell=0}^{\lfloor k/2 \rfloor - 1} \int_0^1 [(t+2\ell)^\gamma - (t+2\ell+1)^\gamma] \cos \pi t \, dt + \int_{2\lfloor k/2 \rfloor}^k t^\gamma \cos \pi t \, dt.$$

The result now follows from (4.4) and the estimate

$$|\vartheta(k)| \leq \frac{3 - 2^{1+\gamma}}{1+\gamma} + \sum_{\ell=1}^{\lfloor k/2 \rfloor - 1} \{(2\ell)^\gamma - (2+2\ell)^\gamma\} \leq \frac{3 - 2^{1+\gamma}}{1+\gamma} + 2^\gamma.$$

For $\gamma = 0$, the result follows trivially from the definition, as $\mathcal{G}(k) = \int_{-1}^1 e^{\pi i k \rho} \, d\rho = 0$ for all $k \neq 0$.

Now, for $\gamma \in (0, 1], k > 0$, we have

$$\mathcal{G}(k) = -\frac{2\gamma}{\pi k^{1+\gamma}} \int_0^k t^{\gamma - 1} \sin \pi t \, dt. \tag{4.5}$$

An argument analogous to the one used above shows that the integral in (4.5) is bounded by a constant that depends only on γ, thus establishing the result for $\gamma \in (0, 1]$.

Finally, for $\gamma > 1$, the result follows from

$$\mathcal{G}(k) = (-1)^k \frac{2\gamma}{\pi^2 k^2} + \frac{2\gamma(\gamma - 1)}{\pi^2 k^2} \int_0^1 \rho^{\gamma - 2} \cos \pi k \rho \, d\rho.$$

Now, for $g(x) = \log |x|, k > 0$, we observe that

$$\mathcal{G}(k) = \frac{2}{k} \zeta(k), \tag{4.6}$$

where

$$\zeta(k) = \int_0^k \log t \cos \pi t \, dt.$$

Now, the result follows from the following estimate:

$$\begin{aligned} |\zeta(k)| &\leq 1 + \sum_{\ell=1}^{k - \lfloor k/2 \rfloor - 1} \int_0^1 \log \left(\frac{t + 2\ell - (k - 2\lfloor k/2 \rfloor) + 1}{t + 2\ell - (k - 2\lfloor k/2 \rfloor)} \right) dt \\ &\leq 1 + \sum_{\ell=1}^{\infty} \log \left(\frac{2 + 2\ell - (k - 2\lfloor k/2 \rfloor)}{2\ell - (k - 2\lfloor k/2 \rfloor)} \right) = 1 - \log \left(2 - (k - 2\lfloor k/2 \rfloor)\right) \leq 1. \quad \square \end{aligned}$$

We present some examples in Figure 1 to demonstrate that the behavior of $\mathcal{G}(k)$ established in Proposition 4.2 is indeed observed in practice.

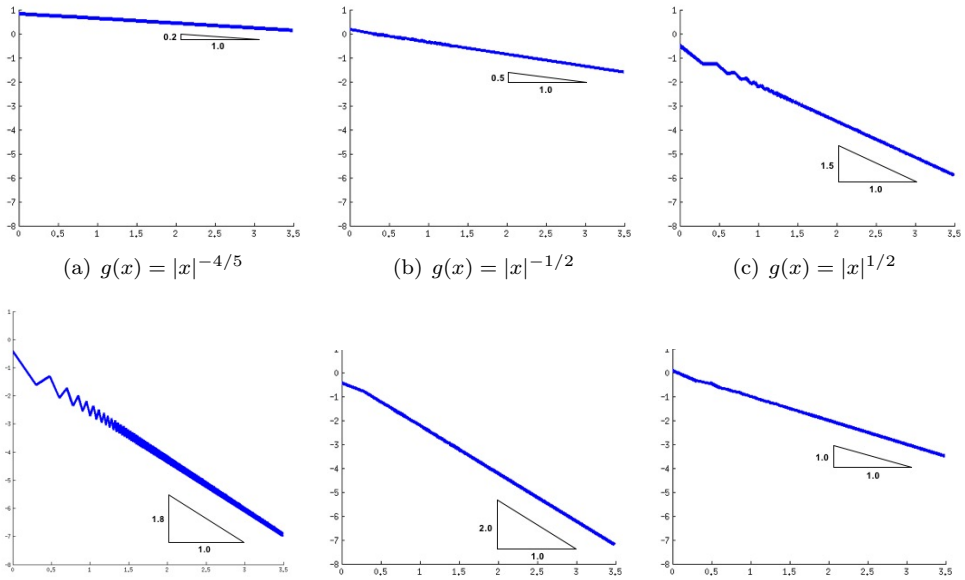

(a) $g(x) = |x|^{-4/5}$ (b) $g(x) = |x|^{-1/2}$ (c) $g(x) = |x|^{1/2}$

(d) $g(x) = |x|^{4/5}$ (e) $g(x) = |x|^3$ (f) $g(x) = \log|x|$

FIG. 1. *Plots showing* $\log_{10}|\mathcal{G}(k)|$ *against* $\log_{10}(k)$ *for kernels of the form* $g(x) = |x|^\gamma$ *for different* γ *values as well as* $g(x) = \log|x|$. *Recall that for the bottom right figure, the expected slope is* -1, *whereas it is* $-\min\{1+\gamma, 2\}$ *for figures with* $g(x) = |x|^\gamma$.

Remark 4.3. The decay rate of $\mathcal{G}(k)$ for kernels of the form $g(x) = g_s(x)g_w(x)$, where g_w is either $g_w(x) = |x|^\gamma, \gamma \in (-1, \infty)$ or $g_w(x) = \log|x|$ with an infinitely differentiable even function g_s, is the same as that of g_w. This follows from the decomposition

$$g(x) = (g_s(x) - g_s(0))g_w(x) + g_s(0)g_w(x),$$

Proposition 4.2, the observation that functions $(g_s(x) - g_s(0))g_w''(x)$, $g_s'(x)g_w'(x)$, and $g_s''(x)g_w(x)$ are absolutely integrable, and that, for $k \neq 0$,

$$\int_0^1 (g_s(x) - g_s(0))g_w(x)\cos\pi kx\,dx = \frac{(-1)^k}{\pi^2k^2}(g_s'(1)g_w(1) + (g_s(1) - g_s(0))g_w'(1)) -$$
$$\frac{1}{\pi^2k^2}\int_0^1 (g_s''(x)g_w(x) + 2g_s'(x)g_w'(x) + (g_s(x) - g_s(0))g_w''(x))\cos\pi kx\,dx.$$

The next result looks at the behavior of how Fourier coefficients decay for the difference between two different extensions of a given function.

LEMMA 4.4. *Let* f_1 *and* f_2 *be two extensions of* $f : [0,1] \to \mathbb{R}$ *that correspond to matrices* $F_1 = (f_{jm}^1)_{0\le j\le 1, 0\le m\le r}$ *and* $F_2 = (f_{jm}^2)_{0\le j\le 1, 0\le m\le r}$, *respectively, that is,*

$$f_1(x) = \begin{cases} f(x), & x \in [0,1], \\ p(F_1)(x), & x \in [-1,0) \end{cases} \quad \text{and} \quad f_2(x) = \begin{cases} f(x), & x \in [0,1], \\ p(F_2)(x), & x \in [-1,0). \end{cases}$$

If F_1 *and* F_2 *are such that their entries satisfy* $f_{jm}^1 = f_{jm}^2 = f^{(m)}(j), j = 0, 1$ *and* $m = 0, \ldots, s$ *for some* $0 \le s \le r$, *then there exists a positive constant* C *such that*

$$|(\widehat{f_1 - f_2})(0)| \le C\|F_1 - F_2\|_{max}, \tag{4.7}$$

$$|(\widehat{f_1 - f_2})(k)| \le C|k|^{-(2+s)}\|F_1 - F_2\|_{max} \tag{4.8}$$

for all $k \neq 0$, where for a matrix $F = (f_{jm})$, $\|F\|_{max} = \max_{jm} |f_{jm}|$.

Proof. If $s = r$, then (4.7) and (4.8) hold with equality as both sides are zero. For $s < r$, the result follows from

$$(\widehat{f_1 - f_2})(0) = \frac{1}{2}\int_{-1}^{0} \left(\sum_{m=0}^{r} (f_{0m}^1 - f_{0m}^2) p_m^0(x) + \sum_{m=0}^{r} (f_{1m}^1 - f_{1m}^2) p_m^1(x) \right) dx$$

and, for $k \neq 0$, from

$$(\widehat{f_1 - f_2})(k) = \frac{1}{2}\int_{-1}^{0} p(F_1 - F_2)(x) e^{-\pi i k x}\, dx =$$

$$\frac{1}{2(-\pi i k)^{s+2}} \sum_{m=0}^{r} \sum_{j=0}^{1} (f_{jm}^1 - f_{jm}^2) \left((p_m^j)^{(s+1)}(0) - (p_m^j)^{(s+1)}(-1) \right) -$$

$$\frac{(-1)^k}{2(-\pi i k)^{s+2}} \sum_{m=0}^{r} \sum_{j=0}^{1} (f_{jm}^1 - f_{jm}^2) \int_{-1}^{0} (p_m^j)^{(s+2)}(x) e^{-\pi i k x}\, dx. \qquad \square$$

The previous lemma thus implies that $(\widehat{u_{c,e} - u_{c,e}^q})(k)$ decays as the rate $|k|^{-2}$. Finally, we arrive at the following upper bound for the numerical integration error.

THEOREM 4.5. *Let $g : \mathbb{R} \to \mathbb{R}$ be an even and absolutely integrable function such that $|\mathcal{G}(k)| \le C_g |k|^{-(1+\gamma)}, k \neq 0$, for constants $C_g > 0$, $\gamma \in (-1, \infty)$, and there exists $n_0 \in \mathbb{N}$ and a constant C_U such that $\|U - U^q\|_{max} \le C_U n^{-q}$ for some $q > 0$ and all $n \ge n_0$. If $u \in C([0,1])$ is such that $|\widehat{u_{c,e}}(k) + \widehat{u_{c,e}}(-k)| \le C_u |k|^{-\delta}, k \neq 0$, for constants $C_u > 0$, $\delta > 1$, then there exists a positive constant C such that, for the sequence of approximations $(A_n u), n \ge n_0$ as defined in (3.4) to Au given in (1.1), we have the error estimate*

$$\|Au - A_n u\|_\infty \le C n^{-\min\{2+q+\gamma, 2+q, \delta, \delta+\gamma\}}.$$

Proof. The result follows from Lemma 4.1 for $-n \le k \le n-1$, $\alpha > 1$, the estimate

$$\sum_{\ell=1}^{\infty} \frac{1}{|k + 2\ell n|^\alpha} \le \frac{2}{(2n)^\delta} \sum_{\ell=1}^{\infty} \frac{1}{\ell^\delta},$$

and

$$\sum_{k=-n}^{n-1} |\mathcal{G}(k)| \le \|g\|_1 + 2C_g \left(1 + \frac{1}{\gamma}\right). \qquad \square$$

We recall that if $u \in C^\infty([0,1])$, then $u_{c,e} \in C^{r,1}([0,1])$ and is piecewise smooth. In this case, for $k \neq 0$, we have

$$|\widehat{u_{c,e}}(k) + \widehat{u_{c,e}}(-k)| \le \begin{cases} C_u |k|^{-(2+r)} & \text{if } r \text{ is even,} \\ C_u |k|^{-(3+r)} & \text{if } r \text{ is odd.} \end{cases}$$

Therefore, the error estimate in Theorem 4.5 reduces to

$$\|Au - A_n u\|_\infty \leq \begin{cases} Cn^{-\min\{2+q+\gamma,2+q,2+r,2+r+\gamma\}} & \text{if } r \text{ is even,} \\ Cn^{-\min\{2+q+\gamma,2+q,3+r,3+r+\gamma\}} & \text{if } r \text{ is odd.} \end{cases}$$

In particular, we note that when $\gamma < 0$, we have

$$\|Au - A_n u\|_\infty \leq \begin{cases} Cn^{-(2+\gamma+\min\{q,r\})} & \text{if } r \text{ is even,} \\ Cn^{-(2+\gamma+\min\{q,1+r\})} & \text{if } r \text{ is odd.} \end{cases}$$

Whereas, for $\gamma \geq 0$, we have

$$\|Au - A_n u\|_\infty \leq \begin{cases} Cn^{-(2+\min\{q,r\})} & \text{if } r \text{ is even,} \\ Cn^{-(2+\min\{q,1+r\})} & \text{if } r \text{ is odd.} \end{cases}$$

Clearly, for a given r, the optimal choice for q, say, q_{opt}, can be made using the prescription

$$q_{opt} = q_{opt}(r) = \begin{cases} r & \text{if } r \text{ is even} \\ r+1 & \text{if } r \text{ is odd,} \end{cases}$$

leading to the convergence rate of $2+r+\min\{0,\gamma\}$ when r is even or $3+r+\min\{0,\gamma\}$ when r is odd.

5. Numerical computation of $\mathcal{G}(k)$. The primary difficulty in the numerical evaluation of $\mathcal{G}(k)$ is due to the kernel singularity at $r = 0$. To overcome this challenge, we use a change of variable of the form $r = \tau^M$ with an odd M. The transformed integral then reads

$$\mathcal{G}(k) = M \int_{-1}^{1} \tau^{M-1} g(\tau^M)) e^{\pi i k \varrho(\tau^M)}\, d\tau.$$

We note that the Jacobian, τ^{M-1} of the transformation renders the integrand $(M-1)$ times continuously differentiable in τ if $g(x) = \log(|x|)$, whereas for $g(r) = |r|^\gamma$, the integrand is M' times continuously differentiable if $\lfloor (1+\gamma)(M+1) \rfloor - 1 \in [M', M'+1)$ for an $M' \in \mathbb{N}$. Thus, the integral defining $\mathcal{G}(k)$ can now be approximated to a high-order accuracy using an appropriate high-order quadrature. For example, in the calculations that we present in this text, we have employed the Clenshaw–Curtis quadrature. For completeness, we recall that the corresponding quadrature points $\{x_j^{cc} : j = 0, \ldots, n_{cc}\}$ and weights $\{\omega_j^{cc} : j = 0, \ldots, n_{cc}\}$ over $[-1, 1]$ are given by

$$x_j^{cc} = \cos\left(\frac{(2j+1)\pi}{2n_{cc}}\right), \quad j = 0, \ldots, n-1$$

and

$$\omega_j^{cc} = \frac{2}{n_{cc}} {\sum_{k=0}^{n_{cc}}}' \vartheta_k \cos\left(\frac{(2j+1)k\pi}{2n_{cc}}\right),$$

where

$$\vartheta_k = \begin{cases} \frac{-2}{k^2-1} & \text{if k is even,} \\ 0 & \text{if k is odd.} \end{cases}$$

TABLE 1

Numerically computed values of $\mathcal{G}(16)$, $\mathcal{G}(256)$, and $\mathcal{G}(1024)$ for various Chenshaw–Curtis quadrature grids of size n_{cc} when $g(x) = \log(|x|)$. The corresponding "exact values," for comparison, are -0.06170905189727761, -0.00097636924521625, and -0.00390315793242324, respectively, which are obtained to 16 digits of accuracy using Mathematica.

n_{cc}	$\beta(16)$	Error
2^6	0.1482838603293570	2.10×10^{-1}
2^7	-0.0565626620038420	5.15×10^{-3}
2^8	-0.0617092489104016	1.97×10^{-7}
2^9	-0.0617090518972840	6.44×10^{-15}
n_{cc}	$\mathcal{G}(256)$	Error
2^9	-0.0251115301421235	2.12×10^{-2}
2^{10}	-0.0154486423047482	1.15×10^{-2}
2^{11}	-0.0039031543234244	3.61×10^{-9}
2^{12}	-0.0039031579323827	4.05×10^{-14}
n_{cc}	$\mathcal{G}(1024)$	Error
2^{11}	0.1270337452551441	1.28×10^{-1}
2^{12}	-0.0290581211042279	2.81×10^{-2}
2^{13}	-0.0009763692620133	1.68×10^{-11}
2^{14}	-0.0009763692454917	2.76×10^{-13}

We demonstrate the effectiveness of this numerical approach through a sequence of computational examples where we compute $\mathcal{G}(k)$ covering a range of k values. In particular, in Table 1, we present a convergence study for the numerical computation of $\mathcal{G}(k)$, where k takes values 16, 256, and 1024, respectively. We observe from these tables that our numerical scheme indeed computes $\mathcal{G}(k)$ with high-order accuracy. As expected, to maintain a desired level in the accuracy across all frequencies, we need to suitably increase n_{cc} with increasing values of k.

6. A discussion on compactly supported integrands and localization. Many important instances of integral operators come with density functions whose support is contained within the domain of integration. A prominent source of such examples is the integral equation formulations of penetrable scattering problem where the material inhomogeneity is localized in a region bounded by a homogeneous surrounding. The proposed integration scheme, when applied to integrals with smooth and compactly supported integrands, simplifies even further. For instance, the extension of u from $[0, 1]$ to $[-1, 1]$ is trivial with the zero polynomial doing the job. Consequently, no correction is required as both $C_L(U)(x)$ and $C_R(U)(x)$ identically take the zero value. The numerical scheme in this case, therefore, reads

$$(A_n u)(x) = \sum_{j=0}^{n-1} w_j^n(x) u_j,$$

where

$$w_j^n(x) = \frac{1}{2n} \sum_{k=-n}^{n-1} \mathcal{G}(k) e^{\pi i k(x-j/n)} \quad \text{with} \quad \mathcal{G}(k) = \int_{-1}^{1} g(r) e^{\pi i k \rho} d\rho.$$

The form that corresponds to (3.3) simply reads

$$(A_n u)(x) = \sum_{k=-n}^{n-1} \mathcal{G}(k) \hat{u}_{c,n}^q(k) e^{\pi i k x}$$

and can be implemented in a straightforward manner using FFT and its inverse using the precomputed $\mathcal{G}(k)$ values. For $u \in C^\infty([0,1])$, the rate of convergence depends directly on the order with which u vanishes at the boundary. A couple of numerical experiments (see Example 7.4) to exemplify this have been included in the next section.

We also point out that, in this context, it is also possible to localize the singular integration using a smooth windowing function, say, η, with the following properties: (a) $\eta : \mathbb{R} \to [0,1]$ is an infinitely differentiable even function, (b) $\eta(0) = 1$, and (c) $\eta(x) = 0$ for all x with $|x| \geq r_0$ for some $r_0 > 0$. Indeed, the integral operator A can be written as

$$(Au)(x) = \int_0^1 g(x-y)\eta(x-y)u(y)\,dy + \int_0^1 g(x-y)(1-\eta(x-y))u(y)\,dy,$$

where the second integral can be approximated to high order in $O(n \log n)$ operations using the classical trapezoidal rule. The first integral, on the other hand, is approximated by

$$\sum_{k=-\infty}^{\infty} \mathcal{G}_\eta(k)\widehat{u_e}(k)e^{\pi i k x} \approx \sum_{k=-n}^{n-1} \mathcal{G}_\eta(k)\widehat{u}^q_{c,n}(k)e^{\pi i k x},$$

where $\mathcal{G}_\eta(k)$ are the localized moments given by

$$\mathcal{G}_\eta(k) = \int_{-r_0}^{r_0} g(\rho)\eta(\rho)e^{\pi i k \rho}\,d\rho.$$

We note that the precomputation of these localized moments is less expensive than their global counterpart due to the relatively small support of the integrand. Additionally, for smoother kernels (for example, $g(x) = |x|^\gamma$ with $\gamma > 1$), having smoothly vanishing integrands leads to faster than quadratic decay rates than are otherwise expected (see Figure 2 for a numerical demonstration).

7. Numerical results. In this section, we demonstrate high-order convergence and accuracy of our quadrature through several computational examples. We compute the numerical order of convergence of our algorithm which relates to the rate at which the error in the approximation of integral decreases as the discretization scale decreases according to the following formula:

$$\text{Order} = \log_2\left(\frac{\max_{0\leq i\leq n}|A(x_i) - A_n(x_i)|}{\max_{0\leq i\leq n}|A(x_i) - A_{2n}(x_i)|}\right). \tag{7.1}$$

The relative error reported in this section is computed as

$$\varepsilon_n = \frac{\max_{0\leq i\leq n}|A_{exact}(x_i) - A_n(x_i)|}{\max_{0\leq i\leq n}|A_{exact}(x_i)|}. \tag{7.2}$$

To corroborate the decay rate, we plot $\log_{10}(\varepsilon_\infty)$ against $\log_{10}(h)$, $h = 1/n$, where the corresponding exact value of the integral is obtained to 16 digits of accuracy using Mathematica whenever it cannot be obtained analytically.

Example 7.1. In the first example, we consider the integral operator A, defined in (1.1), with singular function $g(x) = |x|^\gamma$ and $u(x) = x$. In this case, $(Au)(x)$ can be obtained analytically and is given by

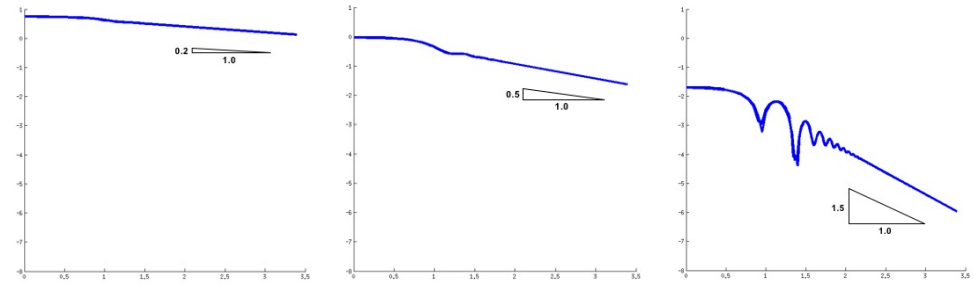

(a) $g(x) = |x|^{-4/5}$ (b) $g(x) = |x|^{-1/2}$ (c) $g(x) = |x|^{1/2}$

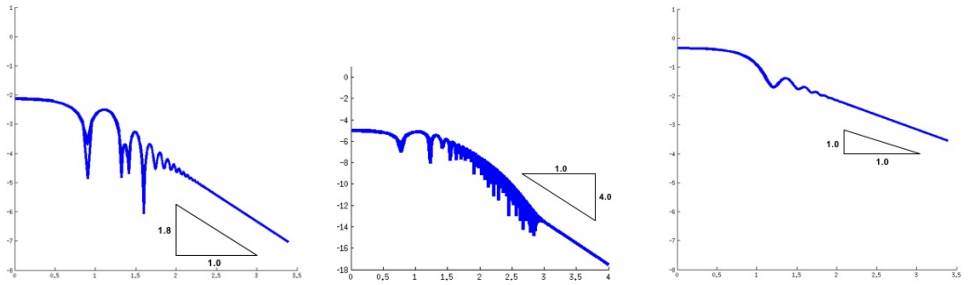

(d) $g(x) = |x|^{4/5}$ (e) $g(x) = |x|^3$ (f) $g(x) = \log|x|$

FIG. 2. *Plots showing* $\log_{10}(|\mathcal{G}_\eta(k)|)$ *against* $\log_{10}(|k|)$ *for kernels of the form* $g(x) = |x|^\gamma$ *for different* γ *values as well as* $g(x) = \log(|x|)$. *Recall that for the bottom right figure, the expected slope is* -1, *whereas it is* $-(1+\gamma)$ *for figures with* $g(x) = |x|^\gamma$.

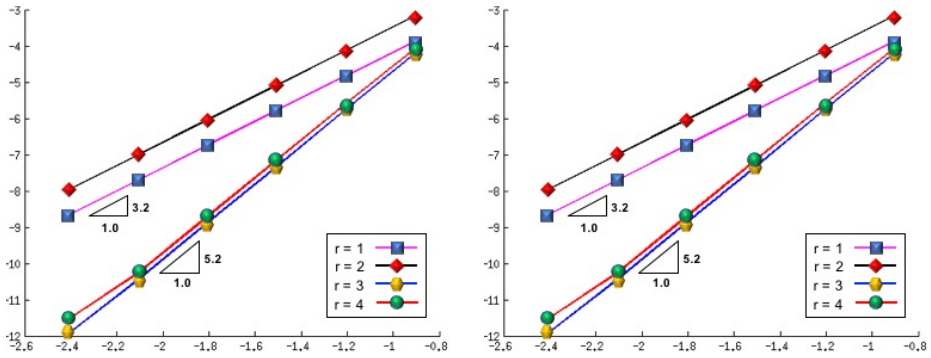

(a) $q = 1$ (b) $q = 3$

FIG. 3. *Plots showing* $\log_{10}(\varepsilon_n)$ *against* $\log_{10}(1/n)$ *for the kernel* $g(x) = |x|^{-4/5}$ *and* $u(x) = x$.

$$(Au)(x) = \frac{x^{2+\gamma}}{2+3\gamma+\gamma^2} + \frac{(1-\gamma)^{1+\gamma}(1+\gamma+x)}{(1+\gamma)(2+\gamma)}. \tag{7.3}$$

We compare the numerically computed integrals with (7.3) when $\gamma = -4/5$. The results have been shown in Figure 3. Note that as $u(x)$ is a linear function, $U^q = U$ for $q \geq 1$. Therefore, there is no effect of the parameter q on the convergence as q increases. To corroborate this, we fix the parameter q at 1 and 3, vary the smoothness parameter r from 1 to 4, and show the corresponding results in Figure 3(a) and Figure 3(b), respectively. These plots clearly demonstrate the effect of r on the convergence rate.

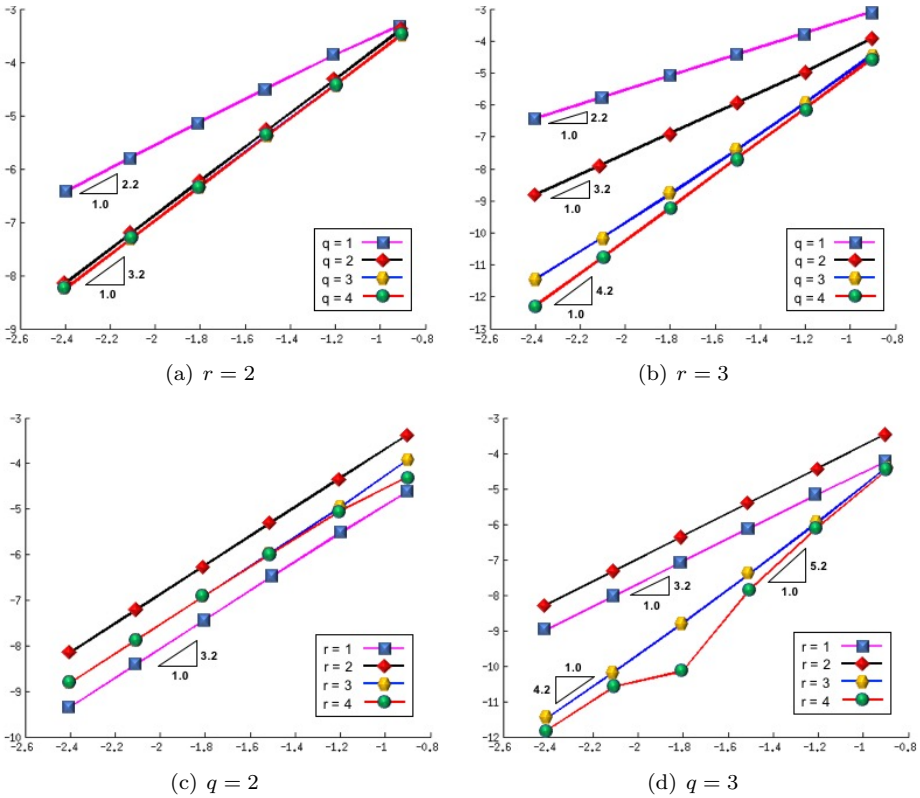

(a) $r = 2$ (b) $r = 3$

(c) $q = 2$ (d) $q = 3$

FIG. 4. *Plots showing* $\log_{10}(\varepsilon_n)$ *against* $\log_{10}(1/n)$ *for* $g(x) = |x|^{-4/5}$ *and* $u(x) = \cos(x)$.

Example 7.2. In the next example, we present the numerical results to demonstrate the effect of smoothness parameter r and order of the boundary derivative approximation q on the convergence of our numerical scheme. We consider the integral operator A, defined in (1.1), with singular function $g(x) = |x|^{\gamma}$, $\gamma = -4/5$ and $u(x) = \cos(x)$. In Figure 4(a) and Figure 4(b), we fix the smoothness parameter at $r = 2$ and $r = 3$, respectively, and vary the parameter q from 1 to 4 in both cases. It can be seen in Figure 4(a) and Figure 4(b) that the integration scheme performs well and the expected order of convergence is achieved in each case. Subsequently, in Figure 4(c) and Figure 4(d), we fix the parameter q and vary the smoothness parameter r to observe its effect on the convergence rate. The plots clearly show that the numerical errors converge as expected.

Example 7.3. Next, we test our numerical integration scheme for some other kernels. We start with $g(x) = \log(|x|)$ and $g(x) = |x|^{\gamma}$, $\gamma = 1/2$. To show the effect of parameter r over the convergence of the integration scheme, we consider $u(x) = x$ and fix q at 1 and vary the smoothness parameter r. It can be seen in Figure 5(a) and Figure 6(a) that the integration scheme performs well and the expected order of convergence is achieved in each case. Next, in Figure 5(b) and Figure 6(b), we consider $u(x) = \cos(x)$ and fix r at 3 and vary q to observe its effect on the convergence rate. These plots clearly demonstrate the effect of q on the convergence rate.

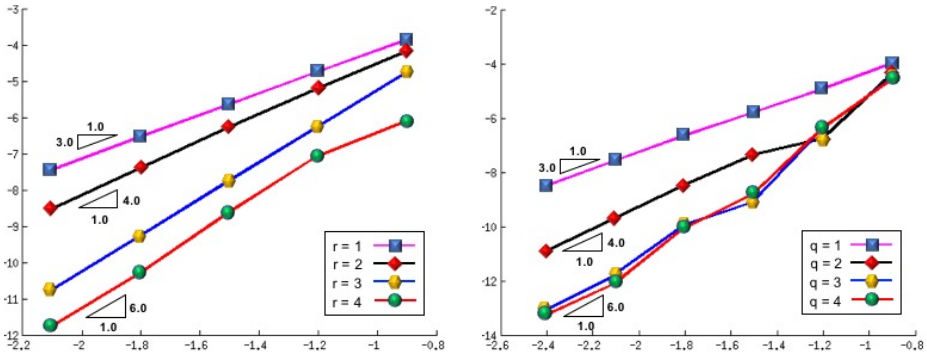

(a) $q = 1$, $u(x) = x$ (b) $r = 3$, $u(x) = \cos(x)$

FIG. 5. *Plots showing* $\log_{10}(\varepsilon_n)$ *against* $\log_{10}(1/n)$ *for the kernel* $g(x) = \log(|x|)$.

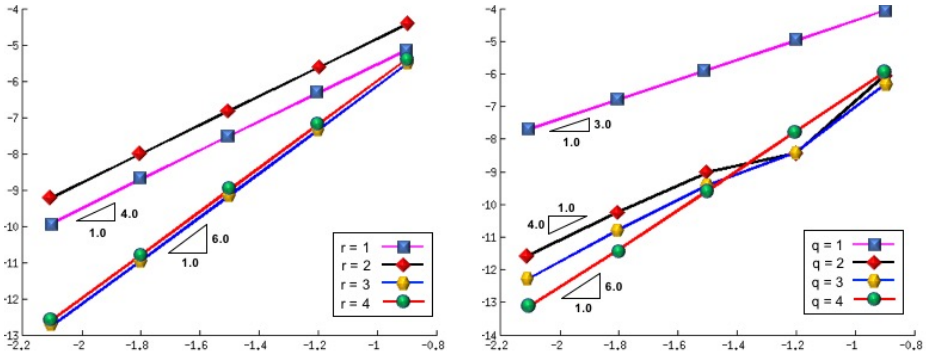

(a) $q = 1$, $u(x) = x$ (b) $r = 3$, $u(x) = \cos(x)$

FIG. 6. *Plots showing* $\log_{10}(\varepsilon_n)$ *against* $\log_{10}(1/n)$ *for the kernel* $g(x) = |x|^{1/2}$.

Finally, the numerical experiments in Figure 7 show the convergence of errors for weakly singular kernels $g(x) = Y_0(|x|)$ (the 0th-order Bessel function of the second kind) and $g(x) = \log(4\sin^2(x/2))$ where for each r, $q = q_{opt}(r)$ is chosen for obtaining the corresponding optimal convergence rate.

Example 7.4. We now demonstrate the performance of our numerical integration scheme for functions whose support is contained in $[0, 1]$. Toward this, we first consider $u(x) = \exp\left(-(\frac{x-x_0}{\sigma})^2\right)$ with $x_0 = 0.5$ and $\sigma = 0.01$. As u vanishes to high order at boundary points $x = 0$ and $x = 1$, the numerical scheme exhibits a super algebraic convergence as seen in Figure 8. We note that this is in contrast to the methodology used in [36] where the expected rate of convergence is algebraic for similarly compactly supported integrands. Finally, to demonstrate the effect of smoothness parameter r on the rate of convergence, we choose a smooth compactly supported function $u = x^3(1-x)^3$ that satisfies $u^{(\ell)}(0) = 0 = u^{(\ell)}(1)$ for $\ell < 3$. The corresponding convergence study is shown in Figure 9.

Example 7.5. We now study the impact of large boundary derivatives on the accuracy of our numerical integration scheme. It can be seen that the size of the polynomial $p(U)(x)$ grows with $\|U\|_{\max}$, and, in fact, for $x \in [-1, 0]$, we have

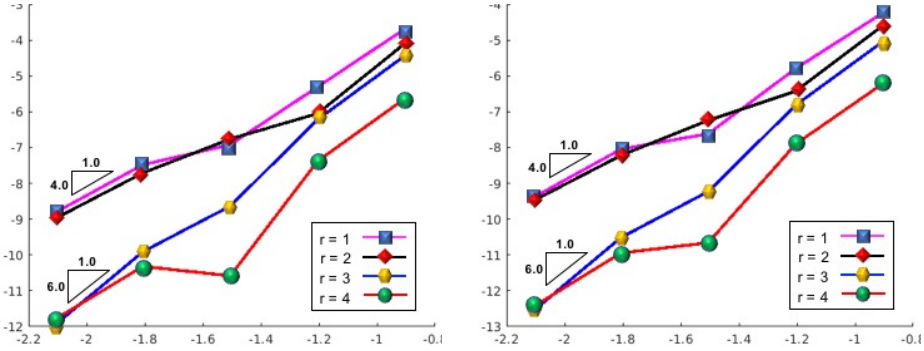

(a) $g(x) = Y_0(|x|), u(x) = x$ (b) $g(x) = \log(4\sin^2(x/2)), u(x) = \cos x$

FIG. 7. *Plots showing* $\log_{10}(\varepsilon_n)$ *against* $\log_{10}(1/n)$.

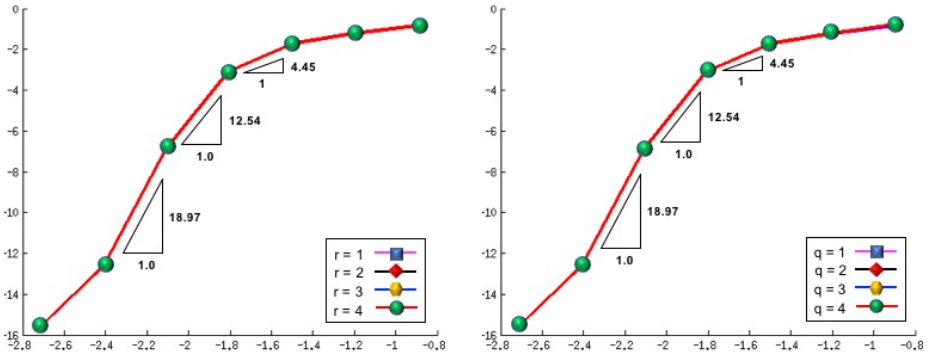

(a) $q = 1$ (b) $r = 3$

FIG. 8. *Plots showing* $\log_{10}(\varepsilon_\infty)$ *against* $\log_{10}(h)$, $h = 1/n$ *for the kernels* $g(x) = |x|^\gamma$, $\gamma = -1/2$ *and* $u(x) = e^{-(\frac{x-0.5}{\sigma})^2}$, *with* $\sigma = 0.01$.

$$|p(U)(x)| \leq 2\binom{2r+2}{r}\|U\|_{\max}.$$

Thus, while the errors in the numerical calculations reach machine precision, say, ϵ_{mach}, relative to $\|U\|_{max}$, their values relative to $\|u\|_\infty$ are not expected to go below $O(\epsilon_{mach}\|U\|_{max}/\|u\|_\infty)$, resulting in a loss of some significant digits. This is particularly exacerbated when the derivative data U has large entries. It is expected that the number of lost digits will be proportional to $\log_{10}(\|U\|_{\max}/\|u\|_\infty)$. To demonstrate this, we take $u(x) = 1/(x+\delta)$ with a small enough $\delta > 0$, where $\|U\|_{\max} = r!\delta^{-(r+1)}$ if smoothness parameter r is used for extension. In particular, if we take $\delta = 10^{-k}$, we expect to roughly loose kr significant digits. As seen in Figure 10, the number of accurate digits beyond which the errors do not improve decreases roughly by k when r is incremented by 1. We see, however, that the errors relative to $\|U\|_{\max}$ do reach close to the machine precision.

Example 7.6. We now apply our numerical scheme for the solution of a volume integral equation that models the one-dimensional inhomogeneous scattering problem that reads

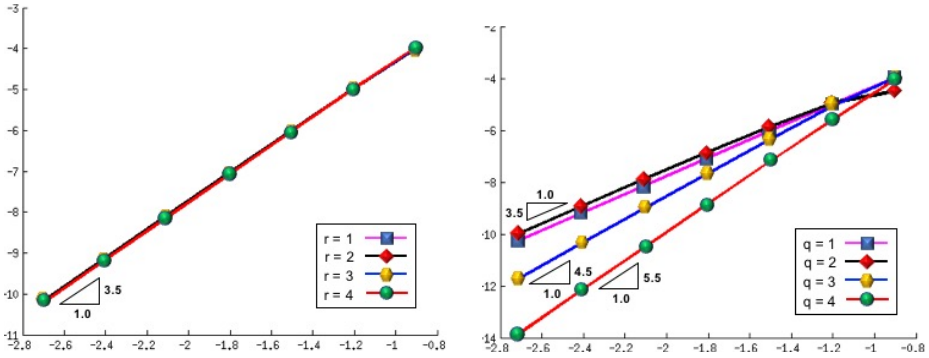

(a) $q = 1$ (b) $r = 3$

FIG. 9. *Plots showing* $\log_{10}(\varepsilon_\infty)$ *against* $\log_{10}(h)$, $h = 1/n$ *for the kernels* $g(x) = |x|^{-1/2}$ *and* $u(x) = (x(1-x))^3$.

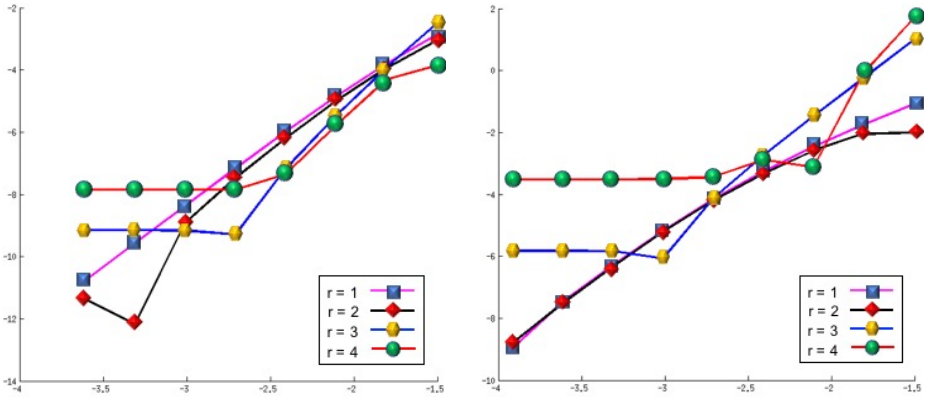

(a) $\delta = 10^{-2}$ (b) $\delta = 10^{-3}$

FIG. 10. *Loss of significant digits due to large boundary derivatives – plots showing* $\log_{10}(\varepsilon_n)$ *against* $\log_{10}(1/n)$ *for the kernel* $g(x) = |x|^{1/2}$ *and* $u(x) = 1/(x+\delta)$ *on* $[0,1]$.

$$u(x) + \kappa^2 \int_0^1 g(x-y)m(y)u(y)\,dy = u_{inc}(x),$$

where $g(x) = \exp(i\kappa|x|)/2\kappa i$, m is the contrast function for the inhomogeneity with $m(x) = 0$ for $x \notin [0,1]$, and u_{inc} is the incoming wave satisfying $u''_{inc} + \kappa^2 u_{inc} = 0$ in $\mathbb{R}$. Writing the integral operator as

$$A(mu)(x) = \frac{\kappa}{2}\left(\int_0^1 \sin\kappa|x-y|m(y)u(y)\,dy - i\int_0^1 \cos\kappa|x-y|m(y)u(y)\,dy\right),$$

we see that the kernels in first and second integrals correspond to $\gamma = 1$ and $\gamma = 0$, respectively, and can be approximated using our Fourier extension based quadrature to high order. This can be seen in Table 2 for a couple of instances where we assume $m \equiv -1$ in $[0,1]$ and take u to be the plane wave $u(x) = \exp i\kappa x$. The convergence study in the left table corresponds to $\kappa = 1$, whereas the one in the right table is for $\kappa = 100$. The errors reported in Table 2 are obtained as $\max_{0\le j\le n} |A(mu)(x_j) - A_n(mu)(x_j)|$,

TABLE 2

A convergence study for the approximation of integral $A(mu)$ for the scattering problem considered in Example 7.6 *where the kernel is* $\exp(i\kappa|x|)/2\kappa i$ *corresponding to the Fourier extension with parameters* $r = 3$ *and* $q = 4$.

$\kappa = 1$		
N	MaxError	Order
2^3	1.23×10^{-6}	– –
2^4	1.72×10^{-8}	6.16
2^5	2.46×10^{-10}	6.12
2^6	3.78×10^{-12}	6.03

$\kappa = 100$		
N	MaxError	Order
2^7	3.78×10^{-7}	– –
2^8	3.52×10^{-9}	6.75
2^9	2.82×10^{-11}	6.96
2^{10}	3.72×10^{-13}	6.25

TABLE 3

A convergence study for the approximation of integral $A(mu)$ for the scattering problem considered in Example 7.6 *where the kernel is* $\exp(i\kappa|x|)/2\kappa i$. *The approximation uses zero extension of the plane wave density mu, that is,* $(mu)_c(x) = -\exp(i\kappa x)$ *on* $[0, 1]$ *and* 0 *otherwise.*

$\kappa = 1$.		
N	MaxError	Order
2^3	1.58×10^{-3}	– –
2^4	3.95×10^{-4}	2.00
2^5	9.89×10^{-5}	2.00
2^6	2.47×10^{-5}	2.00
2^7	6.18×10^{-6}	2.00
2^8	1.55×10^{-6}	2.00
2^9	3.86×10^{-7}	2.00

$\kappa = 100$.		
N	MaxError	Order
2^3	2.16×10^{-3}	– –
2^4	2.80×10^{-5}	6.27
2^5	6.36×10^{-6}	2.14
2^6	1.56×10^{-6}	2.03
2^7	3.87×10^{-7}	2.01
2^8	9.67×10^{-8}	2.00
2^9	2.42×10^{-8}	2.00

where the exact integral $A(mu)(x)$ is given by

$$A(mu)(x) = \frac{1}{4\pi^2}\left(2\kappa i x \exp(i\kappa x) + \exp(-i\kappa x)\left(\exp(2\kappa i) - \exp(2\kappa i x)\right)\right).$$

Clearly, the expected numerical order of convergence corresponding to Fourier extension parameters $r = 3$ and $q = 4$ is achieved in these experiments.

It is interesting to note that the numerical solution of volume integral equations using Fourier smoothing techniques (see [31, 10]) where integrands are extended outside the domain of integration by zero data prior to the Fourier approximation, in our setting, is equivalent to extending the function $m(x)u(x)$ by the zero polynomial. Indeed, when we solve the one-dimensional scattering problem with zero extension, in contrast to rates seen in Table 2, we observe the expected second-order convergence (see Table 3).

8. Summary and conclusions. In this paper, we have proposed a simple, efficient, and high-order numerical integration scheme for the evaluation of the integral of the form

$$(Au)(x) = \int_0^1 g(x - y)u(y)dy$$

with a weakly singular kernel g utilizing the Fourier extension of $u(x)$. The preeminent motivation for this Fourier extension based integration scheme is to compute integral operator A with high-order accuracy in $O(n \log n)$ operations. This text contains a full error analysis of the numerical integration scheme as well as a range of numerical experiments. The results show a clear agreement between the theoretical rates

and the observed ones. As a special case, we also discuss our numerical integration scheme when the integrand has its support contained in the domain of integration and observe that the scheme simplifies even further from the implementation point of view while maintaining the computational accuracy and efficiency. In fact, when u is smooth and compactly supported, the simplified approximation procedure yields superalgebraic convergence. In the general case, the loss of superalgebraic convergence to arbitrarily high convergence rates accompanies the upside that the method requires only $O(n \log n)$ operations.

REFERENCES

[1] B. Adcock, D. Huybrechs, and J. Martin-Vaquero, *On the numerical stability of Fourier extensions*, Found. Comput. Math., 14 (2014), pp. 635–687.

[2] J. Aguilar and Y. Chen, *High-order corrected trapezoidal quadrature rules for functions with a logarithmic singularity in* 2-*d*, Comput. Math. Appl., 44 (2002), pp. 1031–1039.

[3] J. Aguilar and Y. Chen, *High-order corrected trapezoidal quadrature rules for the Coulomb potential in three dimensions*, Comput. Math. Appl., 49 (2005), pp. 625–631.

[4] N. Albin and O. P. Bruno, *A spectral FC solver for the compressible Navier–Stokes equations in general domains* I: *Explicit time-stepping*, J. Comput. Phys., 230 (2011), pp. 6248–6270.

[5] F. Amlani and O. P. Bruno, *An FC-based spectral solver for elastodynamic problems in general three-dimensional domains*, J. Comput. Phys., 307 (2016), pp. 333–354.

[6] B. K. Alpert, *Hybrid Gauss-trapezoidal quadrature rules*, SIAM J. Sci. Comput., 20 (1999), pp. 1551–1584.

[7] A. Averbuch, L. Vozovoi, and M. Israeli, *On a fast direct elliptic solver by a modified Fourier method*, Numer. Algorithms, 15 (1997), pp. 287–313.

[8] J. P. Boyd, *A comparison of numerical algorithms for Fourier extension of the first, second, and third kinds*, J. Comput. Phys., 178 (2002), pp. 118–160.

[9] C. Brezinski, *Extrapolation algorithms for filtering series of functions, and treating the Gibbs phenomenon*, Numer. Algorithms, 36 (2004), pp. 309–329.

[10] O. P. Bruno and E. M. Hyde, *Higher-order Fourier approximation in scattering by two-dimensional, inhomogeneous media*, SIAM J. Numer. Anal., 42 (2005), pp. 2298–2319.

[11] O. P. Bruno and M. Lyon, *High-order unconditionally stable FC-AD solvers for general smooth domains* I. *Basic elements*, J. Comput. Phys., 229 (2010), pp. 2009–2033.

[12] O. P. Bruno, Y. Hana, and M. M. Pohlman, *Accurate, high-order representation of complex three-dimensional surfaces via Fourier continuation analysis*, J. Comput. Phys., 227 (2007), pp. 1094–1125.

[13] T. A. Driscoll and B. Fornberg, *A Padé-based algorithm for overcoming the Gibbs phenomenon*, Numer. Algorithms, 26 (2001), pp. 77–92.

[14] R. Duan and V. Rokhlin, *High-order quadratures for the solution of scattering problems in two dimensions*, J. Comput. Phys., 228 (2009), pp. 2152–2174.

[15] M. Elghaoui and R. Pasquetti, *A spectral embedding method applied to the advection-diffusion equation*, J. Comput. Phys., 125 (1996), pp. 464–476.

[16] P. P. Ewald, *Die berechnung optischer und elektrostatischer gitterpotentiale*, Ann. Phys., 369 (1921), pp. 253–287.

[17] M. Garbey, *Some applications on the superposition principle with Fourier basis*, SIAM J. Sci. Comput, 22 (2000), pp. 1087–1116.

[18] M. Garbey and D. Tromeur-Dervout, *A new parallel solver for the nonperiodic incompressible Navier–Stokes equations with a Fourier method: Application to frontal polymerization*, J. Comput. Phys., 145 (1998), pp. 316–331.

[19] J. F. Geer, *Rational trigonometric approximations using Fourier series partial sums*, J. Sci. Comput., 10 (1995), pp. 325–356.

[20] J. F. Geer and N. S. Banerjee, *Exponentially accurate approximation to piece-wise smooth periodic functions*, J. Sci. Comput., 12 (1997), pp. 253–287.

[21] J. W. Gibbs, *Fourier's series*, Nature, 59 (1898), p. 200.

[22] J. W. Gibbs, *Fourier's series*, Nature, 59 (1899), p. 606.

[23] D. Gottlieb and C.-W. Shu, *Resolution properties of the Fourier method for discontinuous waves*, Comput. Methods Appl. Mech. Engrg., 116 (1994), pp. 27–37.

[24] D. Gottlieb and C.-W. Shu, *On the Gibbs phenomenon* IV: *Recovering exponential accuracy in a subinterval from a Gegenbauer partial sum of a piecewise analytic function*, Math. Comp., 64 (1995), pp. 1081–1095.

[25] D. Gottlieb and C.-W. Shu, *On the Gibbs phenomenon* V: *Recovering exponential accuracy from collocation point values of a piecewise analytic function*, Numer. Math., 71 (1995), pp. 551–526.
[26] D. Gottlieb and C.-W. Shu, *On the Gibbs phenomenon* III: *Recovering exponential accuracy in a sub-interval from a spectral partial sum of a piecewise analytic function*, SIAM J. Numer. Anal., 33 (1996), pp. 280–290.
[27] D. Gottlieb and C.-W. Shu, *On the Gibbs phenomenon and its resolution*, SIAM Rev., 39 (1997), pp. 644–668.
[28] D. Gottlieb, C.-W. Shu, A. Solomonoff, and H. Vandeven, *On the Gibbs phenomena* 1: *Recovering exponential accuracy from the Fourier partial sum of a non-periodic analytic function*, J. Comput. Appl. Math., 43 (1992), pp. 81–98.
[29] E. Hewitt and R. E. Hewitt, *The Gibbs-Wilbraham phenomenon: An episode in Fourier analysis*, Arch. Hist. Exact Sci., 21 (1979) pp. 129–160.
[30] D. Huybrechs, *On the Fourier extension of nonperiodic functions*, SIAM J. Numer. Anal., 47 (2010), pp. 4326–4355.
[31] E. M. Hyde and O. P. Bruno, *A fast, higher-order solver for scattering by penetrable bodies in three dimensions*, J. Comput. Phys., 202 (2005), pp. 236–261.
[32] S. Kapur and V. Rokhlin, *High-order corrected trapezoidal quadrature rules for singular functions*, SIAM J. Numer. Anal., 34 (1997) pp. 1331–1356.
[33] P. Kolm and V. Rokhlin, *Numerical quadratures for singular and hypersingular integrals*, Comput. Math. Appl., 41 (2001), pp. 327–352.
[34] R. Kress, *A Nyström method for boundary integral equations in domains with corners*, Numer. Math., 58 (1990), pp. 145–161.
[35] M. Lyon, *A fast algorithm for Fourier continuation*, SIAM J. Sci. Comput., 33 (2011), pp. 3241–3260.
[36] O. Marin, O. Runborg, and A.-K. Tornberg, *Corrected trapezoidal rules for a class of singular functions*, IMA J. Numer. Anal., 34 (2014), pp. 1509–1540.
[37] R. Matthysen and D. Huybrechs, *Fast algorithms for the computation of Fourier extensions of arbitrary length*, SIAM J. Sci. Comput., 38 (2016), pp. A899–A922.
[38] R. Matthysen and D. Huybrechs, *Function approximation on arbitrary domains using Fourier extension frames*, SIAM J. Numer. Anal., 56 (2018), pp. 1360–1385.
[39] D. Potts, G. Steidl, and A. Nieslony, *Fast convolution with radial kernels at nonequispaced knots*, Numer. Math., 98 (2004), pp. 329–351.
[40] D. Potts and N. Van Buggenhout, *Fourier extension and sampling on the sphere*, in Proceedings of the 12th International Conference on Sampling Theory and Applications, 2017, pp. 82–86.
[41] V. Rokhlin, *End-point corrected trapezoidal quadrature rules for singular functions*, Comput. Math. Appl., 20 (1990), pp. 51–62.
[42] H. Wilbraham, *On a certain periodic function*, Cambridge Dublin Math. J., 3 (1848), pp. 198–201.
[43] K. Xu, A. P. Austin, and K. Wei, *A fast algorithm for the convolution of functions with compact support using Fourier extensions*, SIAM J. Sci. Comput., 39 (2017), pp. A3089–A3106.